Chapter 3. SEAM3D Code Verification

When transport parameters were identical and biodegradation was ignored, transport of any type of solute in SEAM3D duplicated the MT3D solute in all verification problems described by Zheng (1990). Since these problems involved code comparison to one, two, and three-dimensional analytical transport solutions, the following presentation will focus on the verification of the biodegradation algorithm in SEAM3D. Test cases were devised in which advection, dispersion, and source/sink terms were negligible, so concentration changes depended solely on biodegradation. In each case, the model domain represented a 16 x 16 x 1 m confined aquifer, divided into 16 blocks using 4 x 4 x 1 m spacing. In generating the groundwater flow field, the piezometric surface was maintained horizontal, so $\overline{v}_i$ and q_s were zero in the transport simulations. Transport and biodegradation parameters were identical at all nodes, forcing the concentration gradients to be zero.

In general, analytical solutions for the biodegradation equations (2.5) through (2.10) do not exist because the source/sink terms are coupled to biomass growth, and $\nu_{x,ls,le}$ shows a nonlinear dependence on $\overline{S}_{ls}$, $\overline{E}_{le}$, and $\overline{N}_{ln}$ through the Monod terms in equation (2.19) or (2.25). However, analytical solutions may be obtained if parameters are chosen to prevent biomass growth and to avoid the nonlinear regions of the Monod curve. When the concentration of a limiting factor (C) is much less than its half saturation constant (K^c), the utilization rate (ν) can be described by a first order approximation. If C is much greater than K^c, then the Monod curve asymptotically approaches ν^{max}, and ν becomes zero order with respect to C (see Simkins and Alexander, 1984).

For verification of SEAM3D, parameters were chosen to produce an analytical solution for comparison. Thus, the purpose of each test case was to check the accuracy of the computer code, not to demonstrate realistic growth and utilization behavior. In all cases, the threshold concentrations S^t_{ls}, E^t_{le}, and N^t_{ln} were zero, allowing the actual concentrations and half saturation constants to be used in place of the effective values. In each case, two nutrients were simulated using the multiplication option (equation 2.21), with N_{ln} = 9.0 g m^{-3} initially, and $K^n_{x,ln}$ = 1.0 g m^{-3} The nutrient utilization term ($\psi_{x,ln}$) was zero, so N_{ln} remained constant, and the value

of N_x was constant at 0.81. Inhibition coefficients ($\kappa_{le,li}$) were 81 g m^{-3} (μg g^{-1} for Mn(IV) and Fe(III)), and concentrations of the inhibiting EAs (E_{li}) were 9.0 g m^{-3} (μg g^{-1} for Mn(IV) and Fe(III)). Use coefficients for each E_{li} were always zero, so the value of each inhibition term $\left[\kappa_{le,li} / (\kappa_{le,li} + E_{li})\right]$ in equation (2.20b) was constant at 0.9. Retardation factors were calculated using a linear adsorption isotherm. Additional parameters that were identical in all cases included effective porosity (θ = 0.25), initial biomass concentration (M_x = 0.01 g m^{-3}), and EA product generation coefficient ($\zeta_{x,le}$ = 0.5).

3.1 SEAM3D Code Verification

3.1.1 Substrate Test Case

The substrate test case involved degradation of three substrates (S_{ls}) by methanogens (*x* = 6) utilizing two nutrients. The purpose of this test was to verify proper utilization of multiple substrates having different sorptive properties. Methanogens were chosen to allow the inhibition function (equation 2.20b) to be tested for all EA inhibitors. The governing equation for this test was derived by combining equations (2.5), (2.15), and (2.25) in the $R^{bio}_{sink,ls}$ term of equation (2.1) as follows:

$$\frac{\partial S_{ls}}{\partial t} = -\frac{M_6 \; \nu^{max}_{6,ls,6}}{\theta \; R_{ls}} \left[\frac{S_{ls}}{K^{s}_{6,ls,6} + S_{ls}} \right] N_6 \; I_{6,li} \tag{3.1}$$

As described previously, N_6 and $I_{6,li}$ were forced to be constant over time, with N_6 = 0.81. Methanogens were inhibited by O_2, NO_3^-, Mn(IV), Fe(III), and SO_4^{2-}, so $I_{6,li}$ = 0.5905. The substrate retardation factors were R_1 = 1, R_2 = 2, and R_3 = 3. Since the biomass yield ($Y_{x,ls,le}$) and background death rate ($k^{bk}_{d_x}$) were zero (Table 3.1), M_6 was constant, and only S_{ls} varied with time. Because S_{ls} was much less than $K^{s}_{6,ls,6}$ (Table 3.1), equation (3.1) simplified to

$$\frac{dS_{ls}}{dt} \cong -k_1 \; S_{ls} \tag{3.2}$$

where

$$k_1 = \frac{M_6 \, \nu^{max}_{6,ls,6}}{K^s_{6,ls,6} \, \theta \, R_{ls}} N_6 \, I_{6,li} \quad . \tag{3.3}$$

Predicted concentrations showed close agreement with the analytical solutions (Figure 3.1) for the three values of k_1 (0.00191, 0.00388, and 0.00765 day^{-1}). Since each k_1 incorporated all aspects of the model relevant to substrate utilization, this case provided an adequate test of the code's handling of the process. We emphasize that parameters were selected to impose first order decay for model verification, and they do not represent field or laboratory measurements. In a field situation, microbial growth and limited EA availability can cause actual decay of hydrocarbon substrates to deviate significantly from a first order approximation.

Table 3.1. Parameters for substrate half saturation coefficient ($K^{s}_{x,ls,le}$), electron acceptor half saturation coefficient ($K^{e}_{x,le}$), maximum specific rate of substrate utilization ($\nu^{max}_{x,ls,le}$), background microbial death rate ($k^{bk}_{d_x}$), yield coefficient ($Y_{x,ls,le}$), initial substrate concentration (S_{ls}), and electron acceptor use coefficient ($\gamma_{x,ls,le}$). Values of the EA index *le* were identical to the microbial population index *x*.

Test Case	*x*	*ls*	$K^{s}_{x,ls,le}$	$K^{e}_{x,le}$	$\nu^{max}_{x,ls,le}$	$k^{bk}_{d_x}$	$Y_{x,ls,le}$	S_{ls}	$\gamma_{x,ls,le}$
			($g\ m^{-3}$)	($g\ m^{-3}$)	(day^{-1})	(day^{-1})	($g\ g^{-1}$)	($g\ m^{-3}$)	($g\ g^{-1}$)
Substrate	6	1	800	--	8	0	0	10	0
	6	2	800	--	32	0	0	10	0
	6	3	800	--	96	0	0	10	0
Sulfate	5	1-3	0.001	800	3	0	0	9999	4
Fe(III)	4	1-3	0.001	--	0.212	0	0	9999	40
Microbial Growth	6	1-3	0.001	--	0.0279	0	0.5	9999	0
Growth Limitation	6	1-3	10	--	0.05	0	0.5	20	0
Growth vs. Death	5	1-3	5	5	0.1	--	0.5	5	4

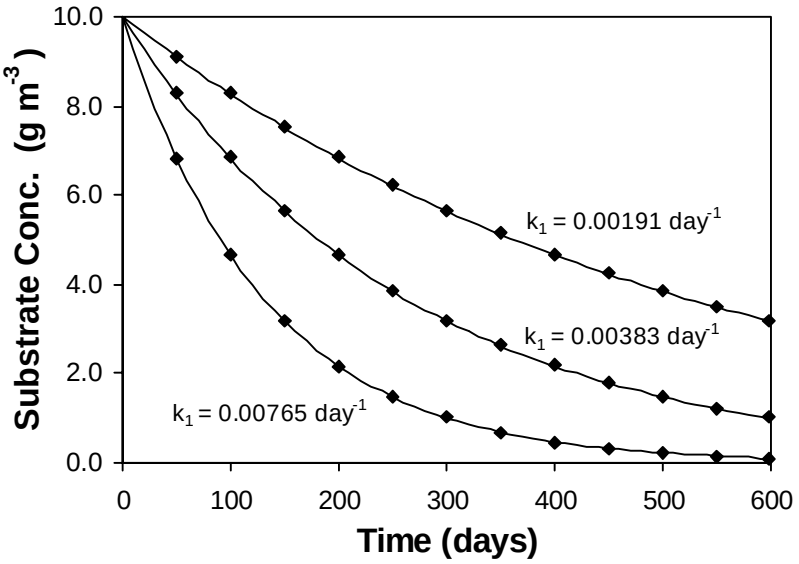

Figure 3.1. SEAM3D predicted substrate concentrations (diamonds) versus analytical solutions (lines) with parameters chosen to impose three rates of first order decay.

3.1.2 Sulfate Test Case

In order to verify utilization of aqueous phase EAs and the creation of products, model parameters were chosen to allow EA utilization by three substrates to follow first order kinetics. All EAs were tested successfully, but only the results for SO_4^{2-} ($x = le = 5$) will be presented here. Equations (2.6), (2.16), and (2.19), were combined in the $R^{bio}_{sink,le}$ term of equation (2.2) to derive a governing equation, which simplified to

$$\frac{dE_5}{dt} \cong -k_1 \, E_5 \tag{3.4}$$

where

$$k_1 = \sum_{ls=1}^{3} \frac{M_5 \, \gamma_{5,ls,5} \, \nu^{max}_{5,ls,5}}{K^e_{5,5} \, \theta} \, N_5 \, I_{5,li} \, . \tag{3.5}$$

The substrate Monod term does not appear in equation (3.5) because S_{ls} was much greater than $K^s_{5,ls,5}$ (Table 3.1), so the term was approximately equal to one. As before, N_5, M_5, and $I_{5,li}$ were forced to be constant over time, with $N_5 = 0.81$. Sulfate reducers were inhibited by O_2, NO_3^-, Mn(IV), and Fe(III), so $I_{5,li} = 0.6561$. The sulfate concentration (E_5) was 9.0 g m^{-3} initially, so E_5 was always much less than $K^e_{5,5}$ (Table 3.1), and the EA Monod term simplified to [E_5 / $K^e_{5,5}$].

For generation of the product H_2S ($lp = 5$), equations (2.2), (2.6), (2.9), and (3.4), were combined in the R^{bio}_{source} term of equation (2.4) to derive a governing equation, which simplified to

$$\frac{dP_5}{dt} \cong k_1 \, \frac{\zeta_{5,5}}{R_5} \, E_5 \tag{3.6}$$

where k_1 is defined by equation (3.5), and R_5 is the H_2S retardation factor. Integration of equation (3.1) gives $E_5 = E^o_5 \exp(-k_1 t)$, where E^o_5 is the initial concentration of SO_4^{2-}. After substitution for E_5, equation (3.5) can be integrated to obtain

$$P_5 \cong -\frac{\zeta_{5,5}}{R_5} \, E^o_5 \left[\exp(-k_1 t) - 1\right] + P^o_5 \tag{3.7}$$

where P_5^o the initial concentration of H_2S. For this test case, R_5 was one and P_5^o was zero. Predicted concentrations of SO_4^{2-} and H_2S show close agreement with the analytical solutions (Figure 3.2), with the generation coefficient $\zeta_{5,5} = 0.5$ causing 9.0 g m^{-3} SO_4^{2-} to produce 4.5 g m^{-3} H_2S.

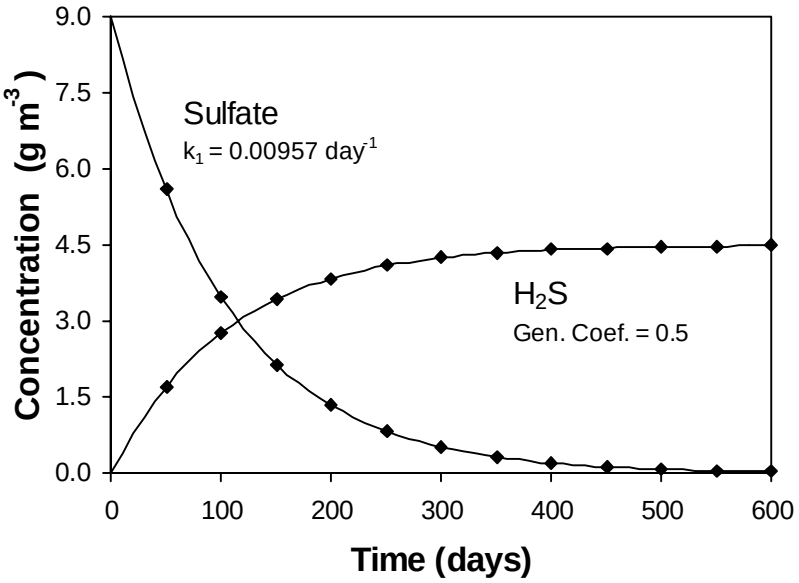

Figure 3.2. SEAM3D predicted SO_4^{2-} and H_2S concentrations (diamonds) versus analytical solutions (lines).

3.1.3 Fe(III) Test Case

To verify model handling of solid phase EAs and their products, parameters were chosen to allow EA utilization by three substrates to follow zero order kinetics. Both Fe(III) and Mn(IV) were tested successfully, but only the results for Fe(III) (x = le = 4) will be presented here. Equations (2.16) and (2.25) were combined in equation (2.17) to derive a governing equation, which simplified to

$$\frac{dE_4}{dt} \cong -k_0 \tag{3.8}$$

where

$$k_0 = (1\times 10^6)\sum_{ls=1}^{3} \frac{M_4\ \gamma_{4,ls,4}\ \nu_{4,ls,4}^{max}}{\rho_b} N_4\ I_{4,li}\ , \tag{3.9}$$

and the factor of (1 x 10^6) converts μg to g. As before, N_4, M_4, and $I_{4,li}$ were forced to be constant over time, with N_4 = 0.81. Fe(III) reducers were inhibited by O_2, NO_3^-, and Mn(IV), so $I_{4,li}$ = 0.729. The initial concentration of Fe(III) was 210 μg g^{-1}, the threshold concentration was 10 μg g^{-1}, and ρ_b was 1.5 g cm^{-3}. As before, the substrate Monod term does not appear in equation (3.9), because S_{ls} was much greater than $K_{4,ls,4}^s$ (Table 3.1). For generation of the product Fe(II) (lp = 4), equations (2.9), (2.17) and (3.8), were combined in the R_{source}^{bio} term of equation (2.4) to derive a governing equation, which simplified to

$$\frac{dP_4}{dt} \cong \frac{k_0}{(1\times 10^6)} \frac{\zeta_{4,4}\ \rho_b}{R_4\ \theta} \tag{3.10}$$

where k_0 is defined by equation (3.9) and R_4 is the Fe(II) retardation factor. In this test case, R_4 was 5.0, and initial P_4 was zero. Predicted concentrations of Fe(III) and Fe(II) show close agreement with the analytical solutions (Figure 3.3).

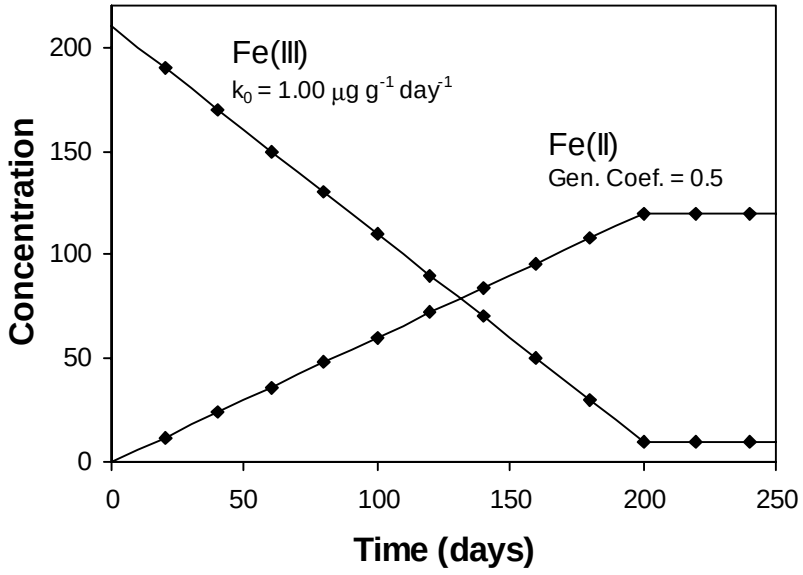

Figure 3.3. SEAM3D predicted Fe(III) and Fe(II) concentrations (diamonds) versus analytical solutions (lines). Units are μg g^{-1} for Fe(III) and g m^{-3} for Fe(II).

3.1.4 Microbial Growth Test Case

Model implementation of microbial growth was verified by choosing parameters to allow methanogens ($x = le = 6$) to grow exponentially on three substrates. Equations (2.25), (2.28), and (2.29) were combined in equation (2.27) to derive a governing equation, which simplified to

$$\frac{dM_6}{dt} \cong k_1 \, M_6 \tag{3.11}$$

where

$$k_1 = -k_{d_6} + \sum_{ls=1}^{3} Y_{6,ls,6} \; \nu_{6,ls,6}^{max} \; N_6 \; I_{6,li} \; . \tag{3.12}$$

As in the substrate test case, N_6 and $I_{6,li}$ were forced to be constant over time, with $N_6 = 0.81$ and $I_{6,li} = 0.6561$. Values for each S_{ls} were much greater than $K^s_{6,ls,6}$ (Table 3.1), so the substrate Monod term dropped out of equation (3.12). Predicted values of biomass concentration M_x show close agreement with the analytical solution (Figure 3.4).

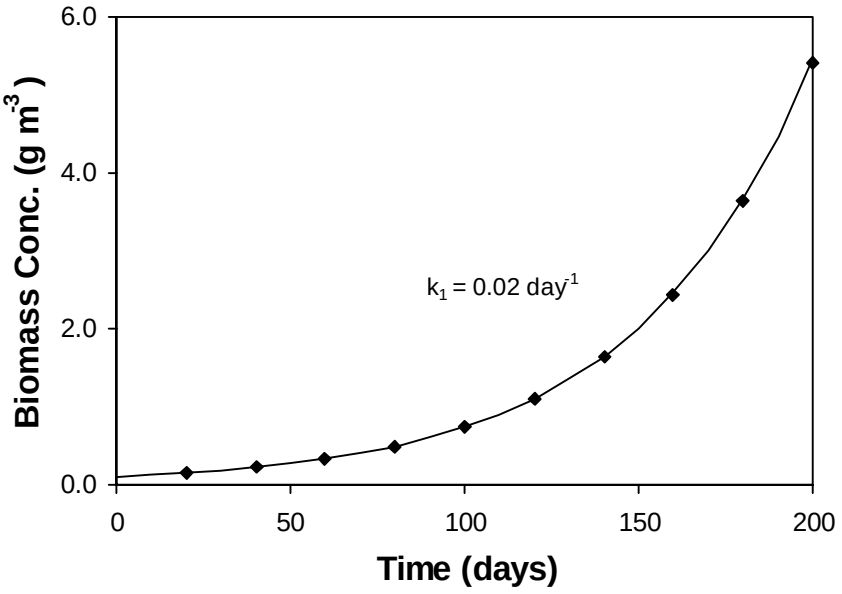

Figure 3.4. SEAM3D predicted biomass concentrations (diamonds) versus analytical solutions (lines) for the microbial growth test case.

3.1.5 NAPL Dissolution Test Case

In order to verify the NAPL dissolution algorithm, model parameters were chosen to allow dissolution of a single substrate to follow first order kinetics. The model domain was 100 x 20 x 20 m, divided into 20 columns, 4 rows, and 4 layers using 5 x 5 x 5 m blocks. Velocity was 0.32 m day^{-1}, and longitudinal dispersivity was 0.5 m. The 16 blocks in the first column (j = 1) contained NAPL source. For each block where NAPL mass existed, the initial NAPL concentration of the substrate ($S_{ls}^{NAPL,0}$) was 9.9 x 10^{-6} g g^{-1}, so the initial NAPL mass of substrate *ls* ($M_{ls}^{NAPL,0}$) was 29.7 kg. The initial NAPL concentration of the tracer ($T_{lt}^{NAPL,0}$) was zero, so the NAPL concentration of inert constituents (I^{NAPL}) was 9.99 x 10^{-3} g g^{-1}. In addition, k^{NAPL} was 0.03 day^{-1}, R_{ls} was 1001, S_{ls}^{sol} was 20,000 g m^{-3}, ω_{ls} and ω_I were 150 g $mole^{-1}$, ρ_b was 1.5 x 10^6 g m^3, and θ was 0.25.

Since $T_{lt}^{NAPL,0}$ was zero and S_{ls}^{NAPL} was always much less than I^{NAPL}, equation (2.13) simplified to

$$f_{ls} = \frac{S_{ls}^{NAPL} / \omega_{ls}}{I^{NAPL} / \omega_I} \quad . \tag{3.13}$$

The large values for R_{ls} and S_{ls}^{sol} allowed S_{ls}^{eq} to be much greater than S_{ls}, so S_{ls} could be omitted from equation (2.11). Equations (2.12) and (2.13) were substituted in equation (2.11) to obtain

$$R_{source,ls}^{NAPL} = k^{NAPL}\left(\frac{S_{ls}^{NAPL} / \omega_{ls}}{I^{NAPL} / \omega_I}\right) S_{ls}^{sol} \tag{3.14}$$

Since transport affected the concentrations at individual blocks, the analytical solution was derived for the total mass of substrate throughout the domain. This allowed changes in NAPL and aqueous phase masses to depend solely on the dissolution rate. For the NAPL, the total mass of substrate (M_{ls}^{NAPL}) was obtained as

$$M_{ls}^{NAPL} = \sum_{j,i,k} \rho_b S_{ls}^{NAPL} \tag{3.15}$$

where j, i, and k are indices for the columns, rows, and layers of the domain. For the aqueous phase, the total mass (M_{ls}) was calculated as

$$M_{ls} = \sum_{j,i,k} \theta S_{ls} \ . \tag{3.16}$$

Equations (3.14) and (3.15) were combined in equation (2.14) to derive a governing equation for the NAPL, which simplified to

$$\frac{dM_{ls}^{NAPL}}{dt} \cong -k_1 \, M_{ls}^{NAPL} \tag{3.17}$$

where

$$k_1 = \frac{\theta}{\rho_b} k^{NAPL} \left(\frac{\omega_I}{I^{NAPL} \omega_{ls}} \right) S_{ls}^{sol} \ . \tag{3.18}$$

For generation of aqueous phase substrate, equations (3.14) and (3.16) were combined in the $R_{source,ls}^{NAPL}$ term of equation (2.1) to derive a governing equation, which simplified to

$$\frac{dM_{ls}}{dt} \cong \frac{k_1}{R_{ls}} M_{ls}^{NAPL} \tag{3.19}$$

where k_1 is defined by equation (3.18). Integration of equation (3.17) gives $M_{ls}^{NAPL} = M_{ls}^{NAPL,0} \exp(-k_1 t)$, where $M_{ls}^{NAPL,0}$ is the initial NAPL mass of substrate. After substituting this expression for M_{ls}^{NAPL}, equation (3.19) can be integrated to obtain

$$M_{ls} \cong -\frac{1}{R_{ls}} M_{ls}^{NAPL,0} \left[\exp(-k_1 t) - 1 \right] + M_{ls}^{o} \tag{3.20}$$

where M_{ls}^{o} is the initial aqueous phase mass of substrate, set to zero for this test case. Predicted concentrations of NAPL and aqueous phase masses show close agreement with the analytical solutions (Figure 3.5).

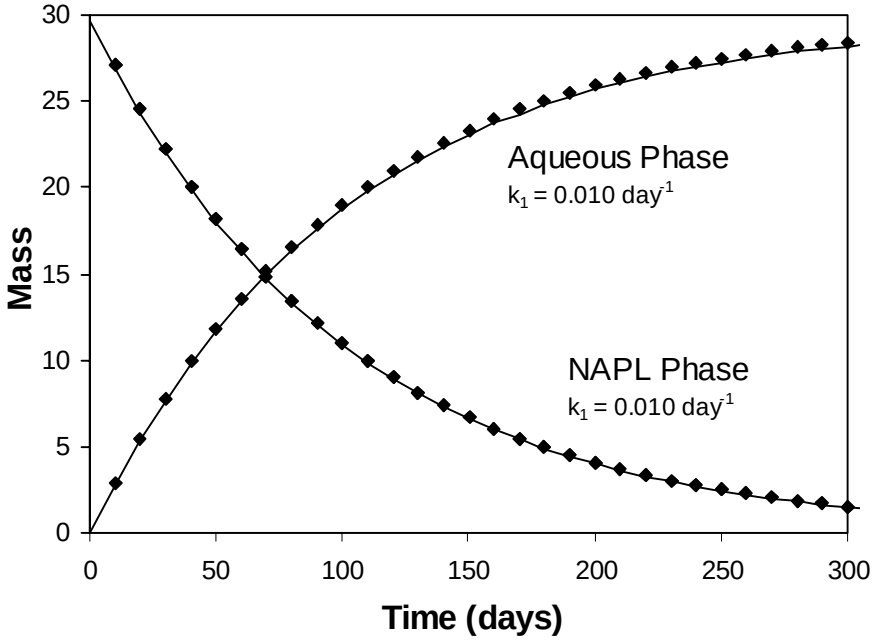

Figure 3.5. SEAM3D predicted NAPL and aqueous phase substrate concentrations (diamonds) versus analytical solutions (lines) for the NAPL dissolution test case. Units are kg for the NAPL and g for the aqueous phase.

3.2 SEAM3D Code Demonstrations

3.2.1 Demonstration of Growth Limitation

The no flow domain from the previous sections was used to demonstrate the method (Section 2.1.4) for microbial growth limitation. Three hydrocarbon substrates were utilized by methanogens, with relevant parameters shown in Table 3.1. The boundary condition for each substrate was constant concentration, which is commonly used to represent a contaminant source zone. When the growth limitation method was not employed, M_x grew exponentially (Figure 3.6) without bound.

The growth limitation method did not affect biomass at early times (Figure 3.6) when ample substrate was available for the microbes. However, by 180 days, M_x had increased to 7.5 g m^{-3}, which is the critical value obtained from equation (2.30). Thus the total substrate concentration did not allow another doubling of the microbes, and the population quit growing. In field scale simulations, substrate, EA, and nutrient availability generally prevent biomass from reaching the critical concentration. However, the critical concentration may be reached at the upgradient edge of a contaminant source zone, where substrate, EA, and nutrients may be abundant for many years. Also, restrictions on microbial growth may be needed to simulate sites where engineered systems provide nutrient and EAs to an aquifer for enhanced bioremediation.

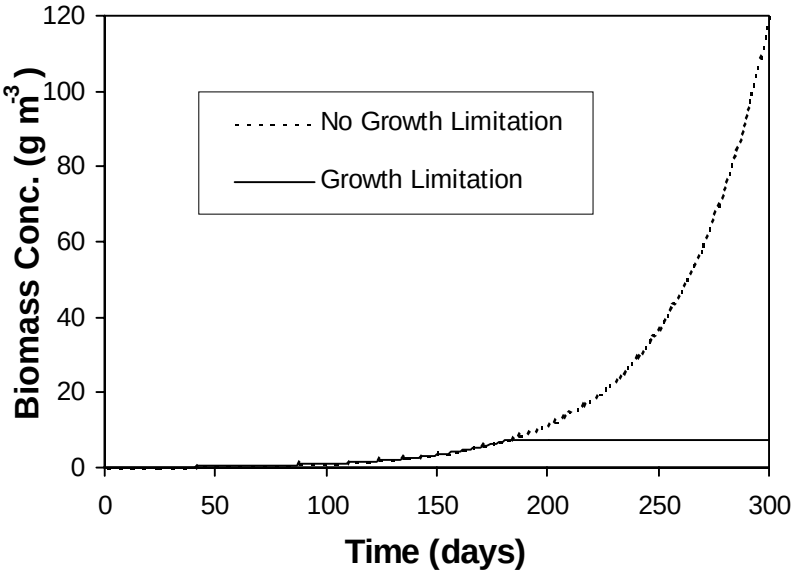

Figure 3.6. SEAM3D predicted biomass concentrations versus time, showing the effect of the growth limitation algorithm.

3.2.2 Demonstration of Microbial Growth versus Death

The no flow domain from the previous sections was used to demonstrate microbial growth as influenced by the effective death term (Section 2.1.4). Three substrates and two nutrients were utilized by SO_4^{2-} reducers, with relevant parameters shown in Table 3.1. Initial concentrations were 9.0 g m^{-1} for SO_4^{2-}, and 0.01 g m^{-1} for biomass. Nutrient initial concentrations were 9.0 g m^{-1}, with $K^n_{x,ln}$ = 5.0 g m^{-3} and $\psi_{x,ln}$ = 4.0. All blocks in the model domain were active for all components. When the effective death term was used, the value for $k^{bk}_{d_x}$ was 0.0133 day^{-1}, and the value of k_{d_x} varied according to equation (2.29). For comparison, additional simulations were performed with k_{d_x} forced to be constant at 0.0, 0.005, and 0.02 day^{-1}.

In the absence of microbial death (k_{d_x} = 0), biomass increased monotonically until EA, and nutrient became depleted (Figure 3.7), with 2.09 g m^{-3} substrate utilized. When k_{d_x} varied, biomass peaked at 230 days, and a total of 1.81 g m^{-3} substrate were utilized. A similar amount of substrate (1.82 g m^{-3}) was utilized when k_{d_x} = 0.005 day^{-1}; however, for k_{d_x} = 0.02 day^{-1}, only 0.349 g m^{-3} were utilized because the growth rate never exceeded the death rate. Thus, biomass concentration simply decreased from its initial value (Figure 3.7).

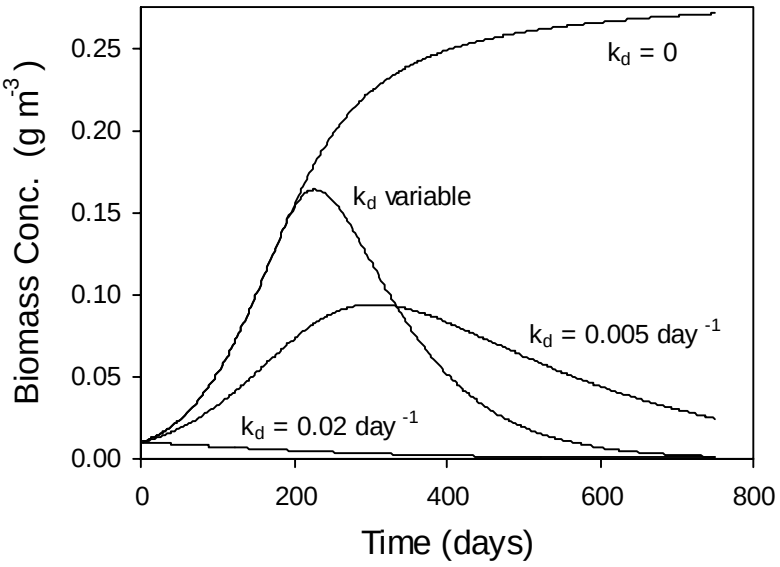

Figure 3.7. SEAM3D predicted biomass concentrations versus time, for various values of the death rate (k_d).

3.2.3 Biodegradation of Five Hydrocarbons

The no flow domain from the previous sections was used to demonstrate utilization of five hydrocarbons (HCs) by O_2, NO_3^-, Fe(III), SO_4^{2-}, and methanogens at various values for ν^{max}. For all EAs and microbial populations, M_x was 0.001 g m^{-3} initially, $\kappa_{le,li}$ was 0.1 g m^{-3} (μg g^{-1} for Fe(III)), $K^s_{x,ls,le}$ was 0.01 g m^{-3}, $K^e_{x,le}$ was 1.0 g m^{-3}, $Y_{x,ls,le}$ was 0.5 g g^{-1}. The small value for $K^s_{x,ls,le}$ caused utilization to be zero order with respect to HC concentration; thus the relative rates of utilization of the five HCs remained constant, even as their concentrations changed. Initial aqueous concentrations were 12 g m^{-3} for all HCs, 8 g m^{-3} for O_2, 40 g m^{-3} for NO_3^-, 90 μg g^{-1} for Fe(III), and 60 g m^{-3} for SO_4^{2-}. EA use coefficients ($\gamma_{x,ls,le}$) were 3.0, 4.0, 40.0, and 4.0 g g^{-1} for O_2, NO_3^-, Fe(III), and SO_4^{2-}, respectively. For the first hydrocarbon (HC1), $\nu^{max}_{x,ls,le}$ was 1.0 day^{-1} for O_2, and 0.5 day^{-1} for all anaerobic processes. These rates were divided in half for each successive hydrocarbon, HC2 to HC5. All HCs were retarded with R_{ls} = 2, and effective porosity was 0.3.

As expected, each HC was utilized twice as fast as its successor; e.g. all 12 g m^{-3} HC1 were used by 61 days, while 6 g m^{-3} HC2 remained (Figure 3.8). The low values for $\kappa_{le,li}$ caused a high degree of inhibition; thus each EA was depleted (Figure 3.9) before utilization of the next EA began. Analysis of the data showed that each EA was utilized correctly according to its use coefficient. Initially, there was sufficient O_2, NO_3^-, Fe(III), and SO_4^{2-} to degrade 37.6 g m^{-3} HC, and 37.7 g m^{-3} were degraded by the time (about 44 days) all four EAs were consumed. Note that due to retardation, the aqueous concentrations in Figure 3.8 reflect only half of the 37.7 g m^{-3} that were degraded. Following the depletion of each EA (shown by the arrows in Figure 3.8), there was a period of slow utilization as the next microbial population grew to a significant level. If the $\kappa_{le,li}$ and initial M_x had been larger, then these periods would have been less pronounced. Nevertheless, an initially small M_x may cause a lag in substrate utilization as the microbes acclimate to the changing availability of EAs.

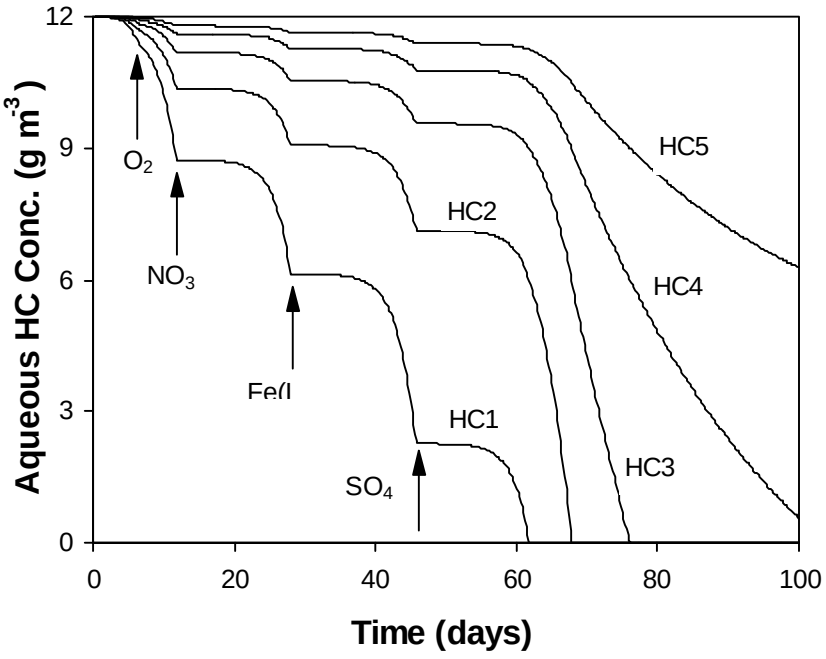

Figure 3.8. SEAM3D predictions of the five hydrocarbon (HC) substrate concentrations, showing the effect of varying the maximum specific rate of substrate utilization ($\nu^{max}_{x,ls,le}$). Arrows indicate the termination of each electron acceptor process.

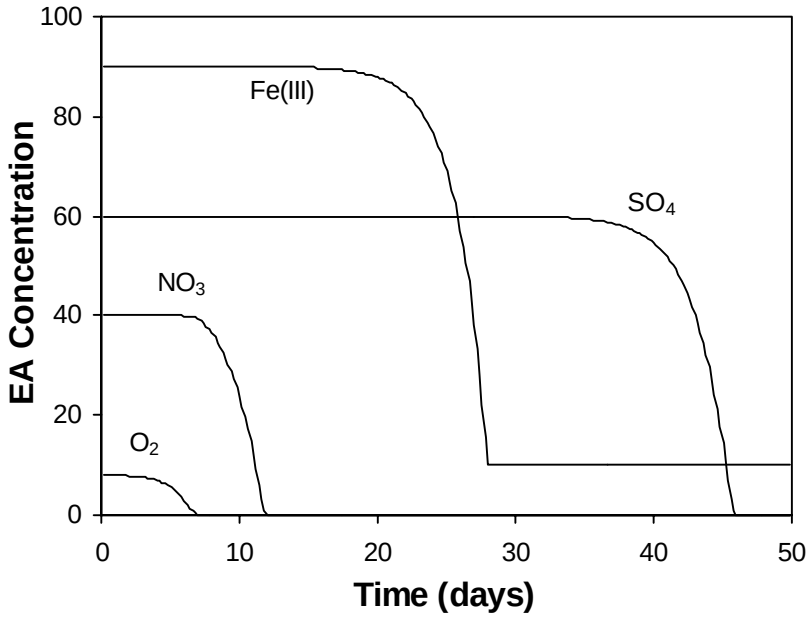

Figure 3.9. SEAM3D predictions of electron acceptor (EA) concentrations, showing that utilization of each EA is inhibited until the preceding EA has been depleted.

3.3 Conclusions

The computer code SEAM3D demonstrated close agreement with analytical solutions for biodegradation of multiple solutes utilizing the entire range of electron acceptors (EAs). Test cases were chosen to verify the major aspects of the biodegradation algorithm, and the results suggest that the computer code correctly implements the model. Demonstration scenarios indicated that the method of linking growth and death rates to concentrations of available substrates, EAs, and nutrients placed reasonable limits on microbial biomass. Although an acclimation period to new substrates is not included in the conceptual model, the effect of microbial acclimation to changing EA availability was shown to cause a lag in utilization.